ARMY RESEARCH LABORATORY

A Modified Zerilli-Armstrong Constitutive Model Describing the Strength and Localizing Behavior of Ti-6Al-4V

by Hubert W. Meyer, Jr.

ARL-CR-0578 **September 2006**

prepared by

Dynamic Sciences, Inc.
1003 Old Philadelphia Road Ste 210
Aberdeen, MD 21001

under contract

DAAD-1702-C0071

Approved for public release; distribution is unlimited.

NOTICES

Disclaimers

The findings in this report are not to be construed as an official Department of the Army position unless so designated by other authorized documents.

Citation of manufacturer's or trade names does not constitute an official endorsement or approval of the use thereof.

DESTRUCTION NOTICE—Destroy this report when it is no longer needed. Do not return it to the originator.

Army Research Laboratory
Aberdeen Proving Ground, MD 21005-5069

ARL-CR-0578 **September 2006**

A Modified Zerilli-Armstrong Constitutive Model Describing the Strength and Localizing Behavior of Ti-6Al-4V

Hubert W. Meyer, Jr.
Weapons and Materials Research Directorate, ARL

prepared by

Dynamic Sciences, Inc.
1003 Old Philadelphia Road Ste 210
Aberdeen, MD 21001

under contract

DAAD-1702-C0071

Approved for public release; distribution is unlimited.

REPORT DOCUMENTATION PAGE

Form Approved
OMB No. 0704-0188

Public reporting burden for this collection of information is estimated to average 1 hour per response, including the time for reviewing instructions, searching existing data sources, gathering and maintaining the data needed, and completing and reviewing the collection information. Send comments regarding this burden estimate or any other aspect of this collection of information, including suggestions for reducing the burden, to Department of Defense, Washington Headquarters Services, Directorate for Information Operations and Reports (0704-0188), 1215 Jefferson Davis Highway, Suite 1204, Arlington, VA 22202-4302. Respondents should be aware that notwithstanding any other provision of law, no person shall be subject to any penalty for failing to comply with a collection of information if it does not display a currently valid OMB control number.

PLEASE DO NOT RETURN YOUR FORM TO THE ABOVE ADDRESS.

1. REPORT DATE *(DD-MM-YYYY)*	2. REPORT TYPE	3. DATES COVERED (From - To)
September 2006	Final	April through December 2005

4. TITLE AND SUBTITLE

A Modified Zerilli-Armstrong Constitutive Model Describing the Strength and Localizing Behavior of Ti-6Al-4V

5a. CONTRACT NUMBER
DAAD-1702-C0071

5b. GRANT NUMBER

5c. PROGRAM ELEMENT NUMBER

6. AUTHOR(S)

Hubert W. Meyer, Jr. (ARL)

5d. PROJECT NUMBER
622618AH80

5e. TASK NUMBER

5f. WORK UNIT NUMBER

7. PERFORMING ORGANIZATION NAME(S) AND ADDRESS(ES)

Dynamic Sciences, Inc.
1003 Old Philadelphia Road Ste 210
Aberdeen, MD 21001

8. PERFORMING ORGANIZATION REPORT NUMBER
ARL-CR-0578

9. SPONSORING/MONITORING AGENCY NAME(S) AND ADDRESS(ES)

U.S. Army Research Laboratory
Weapons and Materials Research Directorate
Aberdeen Proving Ground, MD 21005-5066

10. SPONSOR/MONITOR'S ACRONYM(S)

11. SPONSOR/MONITOR'S REPORT NUMBER(S)

12. DISTRIBUTION/AVAILABILITY STATEMENT

Approved for public release; distribution is unlimited.

13. SUPPLEMENTARY NOTES

The contracting officer's representative (COR) is Todd Bjerke, U.S. Army Research Laboratory, ATTN: AMSRD-ARL-WM-TD, Aberdeen Proving Ground, MD 21005-5069, telephone number (410) 306-0799.

14. ABSTRACT

Modeling localizing behavior (e.g., shear instability) of metals such as Ti-6Al-4V has been an important goal for some time in the study of ballistic impact and penetration phenomena. Toward this end, Zerilli and Armstrong proposed a constitutive model for metals with a hexagonal closely packed crystal structure that addressed the shear instability of some of these materials.

This model was fit to Hopkinson Bar data obtained at strain rates from 1,000 to 50,000 per second. Several modifications of the model were made in order to fit the data better, although the dominant physics-based aspects of the model were not changed. The fit was excellent, with an average error of only 1% in the predicted stress over the range of experimental strains and strain rates.

The modified form of the Zerilli-Armstrong model was installed into the Lagrangian shock-physics code EPIC[1] and tested in a series of simulations. Shear localization was predicted in simulations of two experiments where the phenomenon was observed: a Taylor-Anvil experiment and a ballistic limit velocity ("V_{50}") experiment. Good agreement was obtained as well in simulations of two series of penetration experiments; impact velocities ranged from 1100 m/s to 2000 m/s.

[1]Elastic-Plastic Impact Code

15. SUBJECT TERMS

constitutive model; localization; shear band; Ti-6Al-4V; Zerilli-Armstrong

16. SECURITY CLASSIFICATION OF:			17. LIMITATION OF ABSTRACT	18. NUMBER OF PAGES	19a. NAME OF RESPONSIBLE PERSON
a. REPORT	b. ABSTRACT	c. THIS PAGE			Hubert W. Meyer
UNCLASSIFIED	UNCLASSIFIED	UNCLASSIFIED	SAR	30	19b. TELEPHONE NUMBER (*Include area code*) 410-306-0792

Standard Form 298 (Rev. 8/98)
Prescribed by ANSI Std. Z39.18

Contents

List of Figures iv

List of Tables iv

Acknowledgments v

1. Introduction 1

2. The Modified Zerilli-Armstrong Model 2

3. Calibration of the Model 4

4. The Fit 6

5. Testing the Fit in Simulations 9

5.1 Simulation of Taylor Anvil Experiments 10

5.2 Simulation of a V_{50} Experiment 13

5.3 Simulation of Ti-6Al-4V on Ti-6Al-4V Penetration Experiments 16

5.4 Simulation of the Penetration of the 190W Round Into Ti-6Al-4V 17

6. Conclusion 18

7. Recommendation 18

8. References 19

Distribution List 21

List of Figures

Figure 1. Modified Zerilli-Armstrong model predictions compared to experimental data. 7
Figure 2. Dependence of initial yield on the strain rate. 8
Figure 3. Evaluation of the prediction of the initial yield stress based on the form of the model. 8
Figure 4. Johnson-Cook predictions compared to experimental data. 9
Figure 5. Details of the EPIC simulation of the Taylor anvil test with the use of the modified Zerilli-Armstrong model. 11
Figure 6. Photograph of shear localized Taylor anvil specimen (impact velocity of 205 m/s). .. 11
Figure 7. Predicted strain contours showing incipient strain localization in the Taylor anvil test (t = 11 μs is shown; separation from the anvil occurs at abour 14 μs)..... 12
Figure 8. Localization in the Taylor anvil simulation attained when the value of β_0 and $\dot{\varepsilon}_\beta$ was increased. 13
Figure 9. Sectioned view of the impact crater and remaining plate from a V_{50} experiment (taken from reference (*11*); reprinted by permission)..... 14
Figure 10. Localization and plugging in simulations of V_{50} experiments with the use of equation 9 to model the target..... 15
Figure 11. Nascent localization with the Zerilli-Armstrong bcc model in simulations of V_{50} experiments (1200-m/s impact velocity shown). 16
Figure 12. Simulation results compared to experiment and 3-D CTH with an earlier ZA model..... 17
Figure 13. Axisymmetric EPIC simulation results for the current model compared to experiment and other models. 17

List of Tables

Table 1. Parameters for equation 9 for low cost Ti-6Al-4V. 6
Table 2. Parameters for equation 1 for low cost Ti-6Al-4V. 9
Table 3. Summary of the Taylor anvil experiments and simulations. 10

Acknowledgments

This work was supported in part by a grant of high performance computing (HPC) time from the Department of Defense HPC Center at Aberdeen Proving Ground, Maryland. The author wishes to thank Dan Casem of the U.S. Army Research Laboratory (ARL) for making his data available for this work, and Dan Casem and Dave Kleponis of ARL for many helpful consultations. Frank Zerilli of the Naval Surface Warfare Center, Indian Head Division, provided helpful discussions of the model, and Mike Murphy of the Lawrence Livermore National Laboratory and Scott Schoenfeld of ARL helped to get the Global Local Optimizer process running smoothly.

INTENTIONALLY LEFT BLANK.

1. Introduction

Titanium alloyed with 6% aluminum and 4% vanadium (Ti-6Al-4V) is a material of increasing importance in armor applications for the U.S. Army because of its light weight (compared to steel) and its high strength. The U.S. Army Research Laboratory (ARL) has developed a low cost alternative to the common (but expensive) aircraft-grade Ti-6Al-4V. Extensive Hopkinson Bar tests have been conducted on this low cost material (subsequently referred to as simply Ti-6Al-4V), including Casem's recent experiments at strain rates as great as 50,000/s (*1*), in an effort to understand the material's dynamic behavior. The ultimate goal is to develop a capability to predict the material's strength response during the extreme loading conditions encountered during ballistic impact and penetration. This goal would be achieved if a suitable strength model were established for use in finite element and finite difference shock physics codes, such as EPIC[1] (*2*) and CTH[2] (*3*).

Toward this end, several existing strength models were considered as candidates for calibration with the use of the new Hopkinson Bar data: the Johnson-Cook strength model and the Zerilli-Armstrong series of models. The Johnson-Cook model (*4*) calculates yield strength by the relation

$$Y = \left[A + B\varepsilon^{n}\right]\left[1 + C\ln\dot{\varepsilon}^{*}\right]\left[1 - T^{*m}\right] \tag{1}$$

In equation 1, *A*, *B*, *C*, *n*, and *m* are material constants, ε is the strain, $\dot{\varepsilon}^{*}$ is the non-dimensional strain rate, and *T** is the homologous temperature. This model was found to be inadequate for the Ti-6Al-4V material since it does not model the nonlinear strength behavior (versus the logarithm of strain rate) exhibited by the material and does a poor job of modeling two material characteristics (discussed in more detail later) that are important to predicting localization: the coupling of thermal and rate effects and stress saturation (approaching an asymptotic value or reaching a maximum value) at high strains[3]. Nevertheless, this model was calibrated with Casem's data and tested in simulations of penetration experiments as a reference for comparison. Details are discussed in a later section.

The Zerilli-Armstrong models are physically based, and there are several generations of models. Initially, the model addressed metals with either fcc (face-centered cubic) or bcc (body-centered cubic) crystal structures (*5*,*6*). The yield strength is

$$Y = A + \left[C_1 + C_2\sqrt{\varepsilon}\right]e^{\{-C_3 + C_4\ln\dot{\varepsilon}\}T} + C_5\varepsilon^{n} \tag{2}$$

[1]EPIC, which stands for Elastic-Plastic Impact Code, uses a Lagrangian frame to solve the equations of motion.

[2]CTH, which is not an acronym, uses an Eulerian frame to solve the equations of motion. Both EPIC and CTH are widely used across the defense research and development community to model problems in shock wave propagation.

[3]Unless otherwise noted, the term strain refers to equivalent plastic strain.

in which ε is strain, $\dot{\varepsilon}$ is strain rate, and T is temperature. By appropriate choice of the constants (A, C_1, C_2, C_3, C_4, and C_5), the model is applied to either fcc (C_1=C_5=*0*) or bcc (C_2=*0*) metals. This model was used with success in earlier work (*7*). Zerilli and Armstrong expanded the applicability of the fcc/bcc model by the development of a newer representation for hcp (hexagonal closely packed) metals (*8,9*). Then they extended their hcp model to address shear instability (*10*), an important consideration for Ti-6Al-4V. This more recent hcp form was desired here for two reasons. First, the hcp alpha phase in Ti-6Al-4V dominates the microstructure until transformation to the bcc beta phase occurs at approximately 996 ^{o}C (*11*). Thus, hcp behavior is an important component of the material's ballistic behavior, and hcp behavior can be only approximately described by the fcc/bcc model. Second, a model that would address shear instability and the resultant strain localization was desired for the present effort. This model, calibrated with the new, higher strain rate data, was expected to give better results than were obtained in the earlier work.

2. The Modified Zerilli-Armstrong Model

The localizing strength model proposed by Zerilli and Armstrong (*10*) for the strength of predominantly hcp Ti-6Al-4V is somewhat different from equation 2:

$$Y = C_0 + C_1 e^{-\beta T} + C_2 \sqrt{\varepsilon_r \left(1 - e^{-\varepsilon/\varepsilon_r}\right)}\, e^{-\alpha T} \tag{3}$$

Here, C_0, C_1, and C_2 are material constants, α and β are functions of strain rate (described next), and T is the absolute temperature. The expression under the radical will be referred to as the "strain function". The strain is ε, and the material constant ε_r (named the "recovery strain" by Zerilli and Armstrong), affects the strain at which saturation of the stress is achieved.

The square root comes from theoretical (i.e., ideal) considerations of dislocation motion during the plastic deformation of crystals given by Taylor (*12*). In that work, Taylor concluded that the yield stress depends on the square root of strain (and other factors). The problem with a simple square root function is that the stress will not saturate at high strains in a function of the form $Y = K\sqrt{\varepsilon}$. This type of strain hardening behavior is detrimental if modeling of localization is desired, since localization depends on thermal softening effects overtaking the strain hardening effects. In fact, Ti-6Al-4V does saturate at high strains, so Zerilli and Armstrong replaced the simple strain term in the Taylor strain hardening of earlier models with the strain function in equation 3, which shows saturation at high strains.

The thermal and rate effects are coupled in the exponential terms in equation 3; the parameters α and β are

$$\alpha = \alpha_0 - \alpha_1 \ln \dot{\varepsilon} \tag{4}$$

$$\beta = \beta_0 - \beta_1 \ln \dot{\varepsilon} \tag{5}$$

where α_0, α_1, β_0, β_1 are material constants. Zerilli and Armstrong state that $\dot{\varepsilon}$ is the strain rate, a dimensional quantity. Taking the logarithm of a dimensional quantity is at best awkward, for example, requiring awkward units for the constant β_1. Johnson and Cook's approach to the logarithmic function was to non-dimensionalize the strain rate by a reference strain rate (1/s). Several unsuccessful attempts were made here to include the same approach, but none of the attempts were able to accurately model the data across the wide spectrum of strain rates (although each attempt was accurate near the reference strain rate chosen). Finally, the following approach was adopted (the term $\dot{\varepsilon}_\beta$ is borrowed from Zerilli and Armstrong in reference 8).

This approach does not functionally change equations 4 and 5 but only substitutes a new material constant for one of the original ones. Let

$$\beta_1 = \frac{\beta_0}{\ln \dot{\varepsilon}_\beta} \tag{6}$$

where $\dot{\varepsilon}_\beta$ is a material constant, but since it replaces β_1 in equation 5, the model (equation 3) retains the same number of material constants. The units of β_1 in equation 6 are unchanged from the original form. Substitute equation 6 into equation 5:

$$\beta = \beta_0 \left[1 - \frac{\ln \dot{\varepsilon}}{\ln \dot{\varepsilon}_\beta} \right] \tag{7}$$

Similar reasoning yields the new form for α:

$$\alpha = \alpha_0 \left[1 - \frac{\ln \dot{\varepsilon}}{\ln \dot{\varepsilon}_\alpha} \right] \tag{8}$$

The awkward units of the material constants have been eliminated[4]. For present purposes, strain rate units will be s^{-1}. In practice, this new form was better able than the original form to capture the strain rate effect on the strain hardening for Casem's data set. Importantly, the constants $\dot{\varepsilon}_\alpha$ and $\dot{\varepsilon}_\beta$ have physical significance. When $\dot{\varepsilon}$ is less than $\dot{\varepsilon}_\alpha$, α is positive and the exponential term in equation 3 decreases with increasing temperature. This "thermal softening" (reduction of yield strength with increasing temperature) leads to increased strain, which leads to higher temperatures. This cascade effect may lead to localization. However, if $\dot{\varepsilon}$ is greater than $\dot{\varepsilon}_\alpha$, α is negative and the exponential term in equation 3 *increases* with increasing temperature, and the cascade does not occur. A similar argument applies to $\dot{\varepsilon}_\beta$. Thus, large values of the two (relative to $\dot{\varepsilon}$) are desired for modeling strain localization.

For Casem's data, the square root in equation 3 provided only a fair fit. Since the empirical fits for the Johnson-Cook model, which are found in the literature for various materials, give a

[4]Solving equation 6 for β_0 and substituting that into equation 5 will eliminate the logarithm of a dimensional quantity, but the fits obtained with such a form were not as good as those obtained by the method just described.

variety of values for the exponent of the strain hardening term (n in equation 1), optimization was conducted with the radical replaced by a variable exponent (i.e., an additional material constant). Surprisingly, the constant was repeatedly precisely 1 in a variety of optimization runs[5]. The optimization technique is discussed in the next section. Analysis of equation 3 with an exponent of 1 shows that the algebraic form still saturates at high strain. In fact, the model's ability to capture the saturation of the data at high strain rates was improved over the fit obtained with the square root function. This change also improved the representation of the strain rate effect. The overall fit to the data was greatly improved, and this is quantified later. Therefore, the square root in equation 3 is deleted for the present work.

Thus for Casem's data set, the modified form of the Zerilli-Armstrong hcp strength model is

$$Y = C_0 + C_1 e^{-\beta T} + C_2 \left[\varepsilon_r \left(1 - e^{-\varepsilon / \varepsilon_r} \right) \right] e^{-\alpha T} \tag{9}$$

with β and α described by equations 7 and 8. This function fit Casem's data quite well and is the subject of the remainder of this report.

3. Calibration of the Model

The initial (plastic strain = 0) yield strength of the material at T = 0K is Y_c. Under these conditions, equation 9 reduces to

$$Y = C_0 + C_1 \tag{10}$$

Additional unpublished data describing initial yield behavior of the Ti-6Al-4V at various temperatures from 81 K to 693 K were extrapolated to 0 K with the use of an exponential function of the form of the second term in equation 9. The value of Y_c so obtained was 1356 MPa. Thus, a constraint on the fit of equation 9 is that

$$C_0 + C_1 = 1356 \,\text{MPa} \tag{11}$$

C_0 itself has physical significance; it is the static yield strength of the material (i.e., $\dot{\varepsilon} \to 0$ in equation 9). However, in the present work, C_0 was not obtained by quasi-static yield tests but was fit to the data in the global process described next.

Casem's data, summarized in the next section, consisted of stress-strain curves for five different strain rates[6] from 960/s to 46,400/s. Each of the five data sets was itself an average of several Hopkinson Bar tests. For present purposes, each data set was represented by a discretization of

[5]For example, omitting one of the data sets (e.g., 9585/s) or fitting the initial yield parameters independently before fitting the strain hardening parameters, or adding other material constants, or trying different forms for α and β.

[6]A sixth data set (0.1/s) was available but was not used in the calibration process because this rate is not of primary importance in ballistic problems, and including it would have worsened the fit at the important high strain rates.

the data set into roughly 20 stress-strain pairs taken along the curve between initial yield and failure. An optimum fit of equation 9 to this composite data set was sought. The Global Local Optimizer (GLO) (*13*) was used for this purpose. Through sophisticated mathematics, GLO varies all the parameters of equation 9 (with the exception of C_1, which was eliminated from the optimization process through use of equation 11) in a systematic way and optimizes the predictions of the resulting equation relative to the composite data set by searching for a minimum of a user-defined figure of merit (FOM). Here, the FOM was defined as

$$FOM = \frac{1}{N}\sum_i \frac{1}{M}\sum_j \frac{\left|\sigma_{expt} - \sigma_{calc}\right|}{\sigma_{expt}} \tag{12}$$

in which σ_{expt} is the experimental stress, σ_{calc} is the stress calculated from equation 9, the inner summation (j) is over the $M \approx 20$ stress-strain pairs in each strain rate data set, and the outer summation (i) is over the $N = 5$ strain rate data sets. This FOM (x 100) is actually the average percentage error between the experimental stress and the calculated stress at a strain point. The FOM is an indicator of the quality of the fit to the Hopkinson Bar data and is not necessarily indicative of the model's performance in simulations of ballistic events. The FOM is an indicator of the quality of fit when all strains and strain rates are considered, whereas the important part of a ballistic event may include only a subset of those (that subset taken alone may have a different FOM). A larger consideration is the degree to which Hopkinson Bar experiments model ballistic events.

The GLO fitting process consists of selecting a set of material constants and then marching through each data set from initial yield to failure, calculating the stress at each experimental strain. The temperature increase in moving from one strain to the next is required during this process; it is assumed to be entirely attributable to adiabatic heating from plastic work and is calculated from

$$\Delta T = \frac{\beta}{\rho c_p}\sigma_{i-1}\left[\varepsilon_i - \varepsilon_{i-1}\right] \tag{13}$$

where *i* denotes the current stress-strain pair and *i-1* the previous pair. This implicit scheme is necessary because the temperature must be calculated before the current stress (σ_i) can be calculated. A second order scheme (estimating σ_i from σ_{i-1} and σ_{i-2}) was found to be unnecessary. For the present Ti-6Al-4V work, coefficient $\beta = 0.9$, $\rho = 4424$ kg/m^3, and $c_p = 590$ J/Kg•K. Adiabatic heating was included for all dynamic strain rates (960/s to 46,400/s).

This GLO process was repeated a number of times, with material constants chosen by GLO but guided by constraints set by the user (maximum, minimum, starting value, etc.), until a minimum FOM is reached. After this automated GLO process was completed, a manual search was done in the vicinity of the minimum found by GLO to further refine the solution. Improvement was small but useful.

One final note is worth mentioning. Examination of equation 9 shows that for initial yield (plastic strain = 0), the third term is always zero. Thus, early attempts divided the optimization into fitting the remaining constants (C_0, C_1, β_0, and $\dot{\varepsilon}_\beta$) to just the initial yield information from the five data sets, then holding them fixed while fitting the strain hardening constants. This approach yielded much higher (worse) figures of merit than a global approach, wherein all parameters were allowed to vary at once. The reason for this is that the optimization process was constrained by the (albeit accurate) fit to the initial yield data points, and GLO was not allowed to vary those few points in order to improve the overall fit at all strains. Since the high strain performance of the model is important in ballistic events, a global approach was used.

4. The Fit

The optimization process yielded the set of material constants in table 1 for equation 9, for the low cost Ti-6Al-4V material.

Table 1. Parameters for equation 9 for low cost Ti-6Al-4V.

C_0, MPa	1217	C_2, MPa	3955
C_1, MPa	139	ε_r	0.1877
$\dot{\varepsilon}_\beta$,/s	1.597e4	$\dot{\varepsilon}_\alpha$,/s	8.249e5
β_0, /K	1.591e-2	α_0, /K	7.549e-3

The FOM for this fit was 0.0107 or an average error of only 1.07%. The fit obtained by GLO when an exponent of 1/2 was used (as in equation 3) resulted in a FOM of 0.0151 or about 40% worse than that obtained with an exponent of 1. Importantly, a value of 1/2 led to lower values of $\dot{\varepsilon}_\alpha$ and $\dot{\varepsilon}_\beta$, which is detrimental to the ability of the model to predict localization, as previously discussed (and a quantitative example of this is given in a later section). Plotting the strain function in equation 9 (i.e., exponent = 1) shows that saturation of the function occurs at a strain of about 0.70 for $\varepsilon_r = 0.20$ and at a strain of about 2.00 for $\varepsilon_r = 0.50$.

The fit compared to the discretized data is shown in figure 1. The fit to the 0.1/s data (which was omitted from the FOM calculations as well as the calibration process) is shown for information. Even though 0.1/s was omitted from the fitting process, the model prediction still passes through some of the 0.1/s data points. This indicates that the model's predictions of strain rate hardening and thermal coupling (since adiabatic heating, important at the high rates, is negligible at the low rate) are well represented over the range of the data.

The strain rate effect is shown in figure 2; the bi-linear aspect of the data is apparent. The 9585/s data set is near the critical point of the plot. Since equation 9 is a continuous function, it is not able to closely represent the sharp cusp[7] in the stress in the vicinity of this strain rate. This difficulty is apparent in figure 1, where the fit to the 9585/s curve shows the most error of all the high rates. As if to emphasize the critical nature of this strain rate, even the data show a high degree of variability. The maximum and minimum individual tests are shown as dashed lines in figure 1, and the minimum actually overlaps some lower rate data. The model prediction falls within these limits of the experimental variation. The prediction of initial yield for the 0.1/s case is in error by about 15% in figure 2, but this is not considered a liability for ballistic applications; sufficient accuracy is attained by 10^3/s, and the important processes in ballistic problems typically occur at strain rates greater than that.

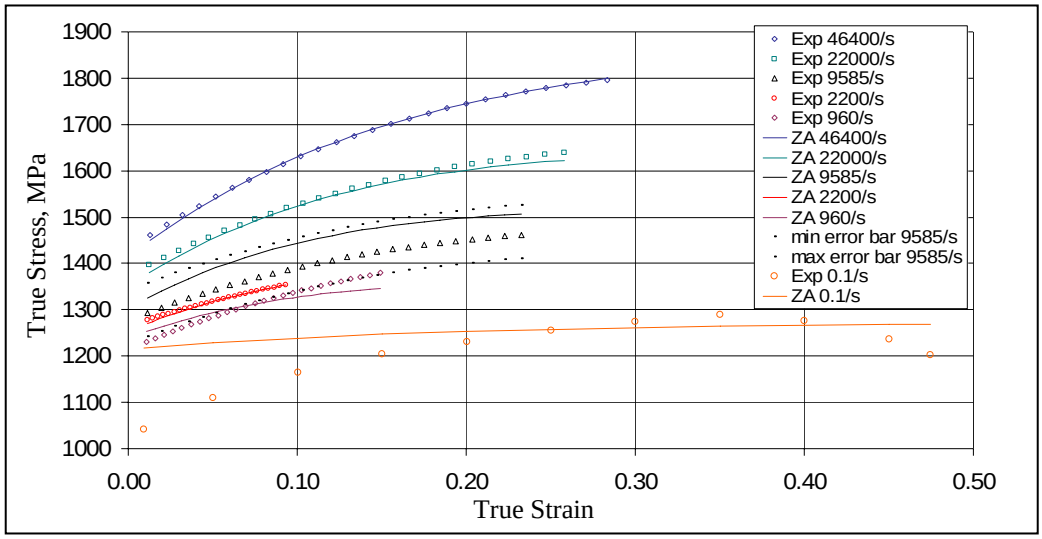

Figure 1. Modified Zerilli-Armstrong model predictions compared to experimental data.

The quality of the fit to the initial yield strength can be examined in another way if predicted initial yield stress is plotted against the exponent of the second term in equation 9 as the independent variable. This exponent provides the functional dependence of initial yield on temperature and strain rate (recall that the third term does not play a role in initial yield strength), but Casem's data are at room temperature (293 K, i.e., no temperature preconditioning and no adiabatic heating for initial yield). Figure 3 shows the comparison; high rate data are at the left. The model captures the data nicely, with the exception of the 0.1/s experiment, seen at the right in the plot.

[7]The cusp is probably continuous in the vicinity of 9585/s, although the slope is changing rapidly. The curve in figure 2 is drawn as discontinuous for simplicity.

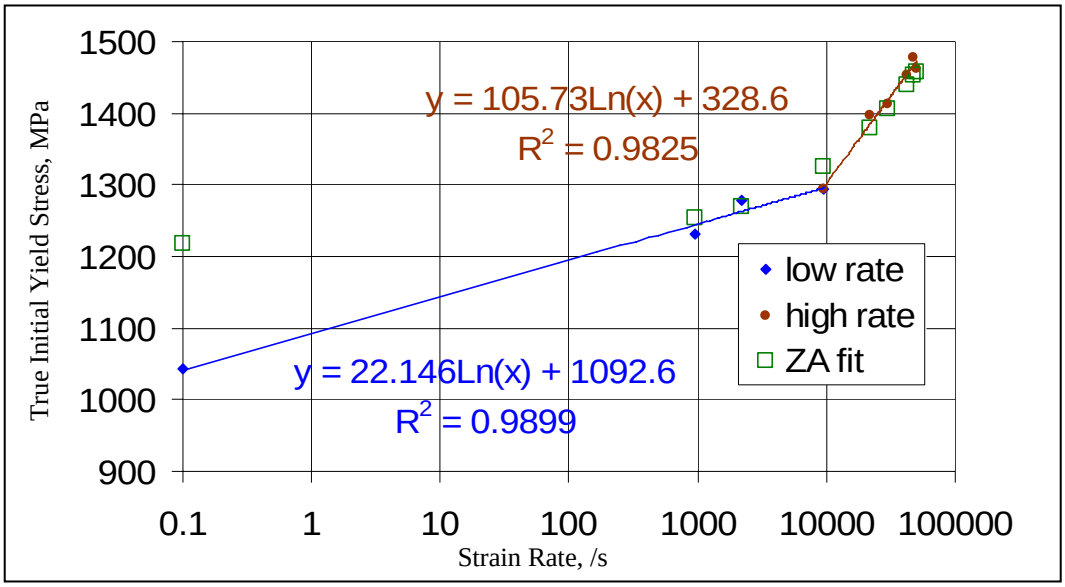

Figure 2. Dependence of initial yield on the strain rate.

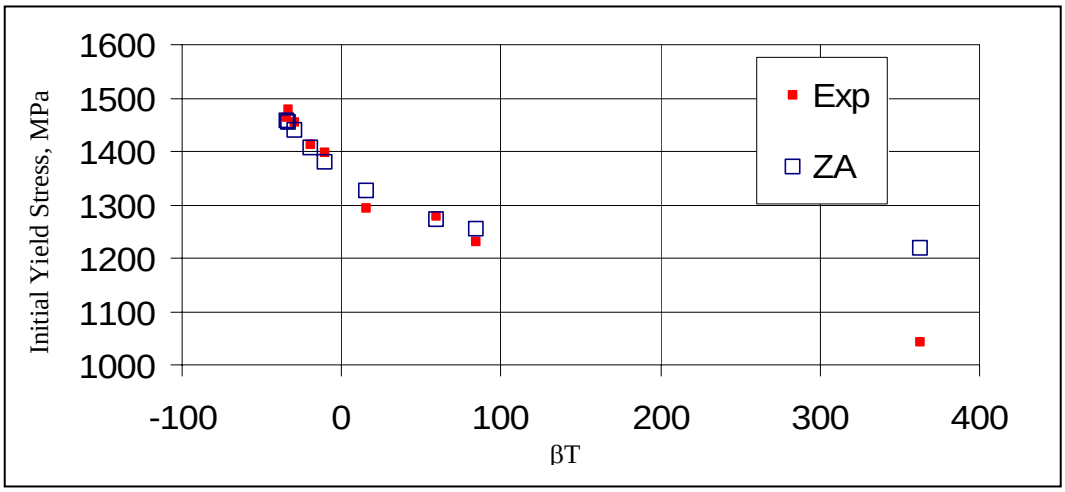

Figure 3. Evaluation of the prediction of the initial yield stress based on the form of the model.

For comparison, the same GLO method was used to fit the Johnson-Cook model to Casem's data. Table 2 gives the resulting material constants for the function in equation 1. The figure of merit for this fit was 0.023 or an average error of 2.3%. Figure 4 shows the performance of the model compared to the experimental data. The Johnson-Cook model allows only a single value for the material constant C in equation 1. Since C is proportional to the slope in figure 2, the single "average" slope of the model allows reasonable predictions for three strain rate curves but misses two of the high strain rate curves. Modifying the model to use a bi-linear slope as in figure 2 improved the fit to the Hopkinson Bar data but provided no improvement in predictions of a Taylor anvil test. As with the modified Zerilli-Armstrong model, the Johnson-Cook model also has trouble with the critical 9585/s rate. Examination of figure 4 also shows that the Johnson-Cook model does not capture stress saturation at high strain as well as the modified

Zerilli-Armstrong model. Interestingly, n = 0.812, close to the exponent of 1 for the strain function in equation 9.

Table 2. Parameters for equation 1 for low cost Ti-6Al-4V.

A, MPa	840
B, MPa	550
C	0.0664
n	0.812
m	1.769

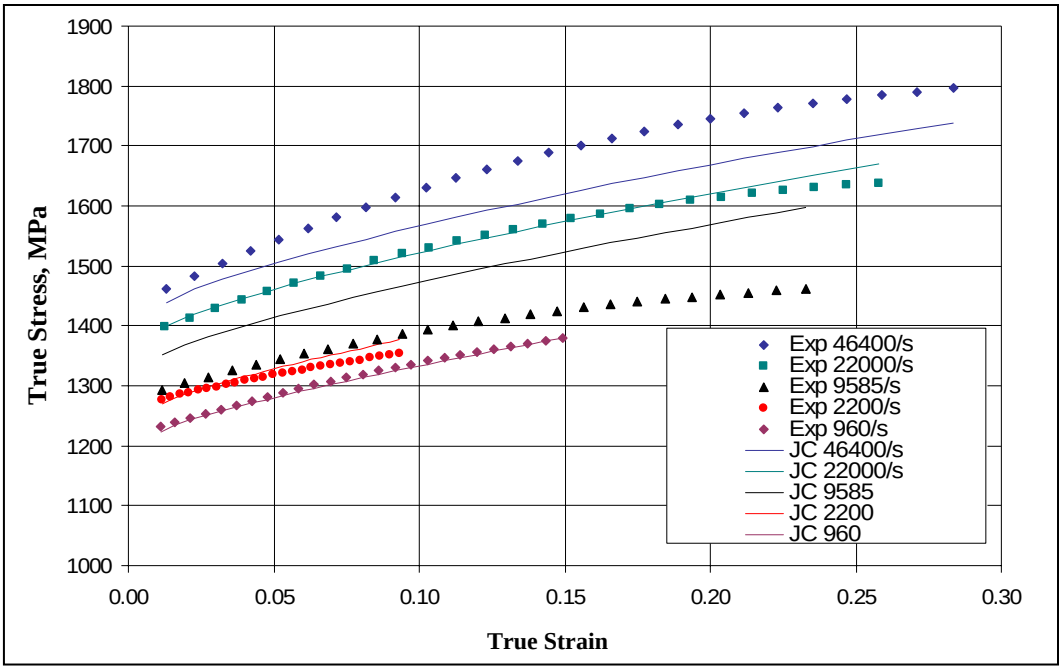

Figure 4. Johnson-Cook predictions compared to experimental data.

5. Testing the Fit in Simulations

Equation 9 and parameters from table 1 were tested in a series of simulations with axisymmetric EPIC. Simulations of four sets of experiments were conducted: Taylor anvil experiments, V_{50} experiments using a steel projectile, penetration of a Ti-6Al-4V penetrator into semi-infinite Ti-6Al-4V, and penetration of a tungsten penetrator into semi-infinite Ti-6Al-4V. All simulations used the Mie Gruneisen equation of state, with EPIC library constants, for all materials. All simulations (except some simulations of the Taylor anvil experiments; see the related footnote in the next section) used the Johnson-Cook fracture model, with EPIC library constants, for all materials. All simulations used EPIC's General Particle Algorithm, except for the Taylor anvil simulations.

5.1 Simulation of Taylor Anvil Experiments

In addition to the Hopkinson Bar experiments, Casem conducted Taylor anvil experiments using specimens fabricated from the low cost Ti-6Al-4V material (*14*). A summary of the results of several experiments at 205 m/s and axisymmetric EPIC simulations (10 crossed elements across the radius of the specimen) with the modified Zerilli-Armstrong model and the Johnson-Cook model is given in table 3. Overall, both models accurately described the final deformed shape of the specimen. Also included in the table is the result of a simulation using the EPIC library parameters for Ti-6Al-4V in the Johnson-Cook model. Those parameters were not intended for the low cost material and are included to satisfy curiosity. Actually, the result is fairly good, although somewhat worse than the models that were calibrated specifically for this material. Finally, for completeness, the prediction of the Zerilli-Armstrong bcc model from reference 7 is included. This bcc model was calibrated with a different set of Hopkinson Bar data[8], one that included strain rates from quasi-static to only 3000/s. Overall, it was slightly less accurate than the present modified Zerilli-Armstrong model for replicating this experiment.

Table 3. Summary of the Taylor anvil experiments and simulations.

	Experiment	**Modified Zerilli-Armstrong**		**Calibrated Johnson-Cook**		**EPIC Johnson-Cook**		**bcc Zerilli-Armstrong**	
	mm	**mm**	**percent error**	**mm**	**percent error**	**mm**	**percent error**	**mm**	**percent error**
Final Length	16.93	16.95	0.1	16.97	0.2	16.31	3.8	16.64	1.7
Maximum Diameter	3.62	3.54	2.2	3.57	1.4	3.94	8.8	3.56	1.7

More details of the EPIC simulation of the Taylor anvil test using the modified Zerilli-Armstrong model are given in figure 5. On the left is a view of the strain field at 14 μs, just after the specimen separates (bounces) from the anvil. In the center is the profile of the specimen at 14 μs. Experimental data points are plotted on the figure, showing quite good agreement between simulation and experiment. The simulation shows a more pronounced effect of the friction at the interface between the specimen and the anvil. On the right in figure 5 is a plot of strain rate at 1 μs when strain rates are generally the highest. It shows that most of the impact end of the specimen is strained at rates of 10^4/s to 10^5/s. However, these high rates are short lived, dropping to a maximum of $2x10^4$/s by 5 μs and continuing to drop rapidly.

Some but not all of the experiments at 205 m/s (nominally) showed shear localization in the specimen; figure 6 shows a typical example. Apparently, this impact velocity is a marginal condition for causing this type of failure. (The experimental results listed in table 3 are average values for two specimens that did not localize.)

[8]The bcc model was not recalibrated with the present Hopkinson Bar data because equation 9 was developed for hcp Ti-6Al-4V and supersedes the bcc model for this material. Alternatively, the Johnson-Cook model makes no such distinction (i.e., it should be applicable to Ti-6Al-4V), so it was calibrated here for comparison purposes.

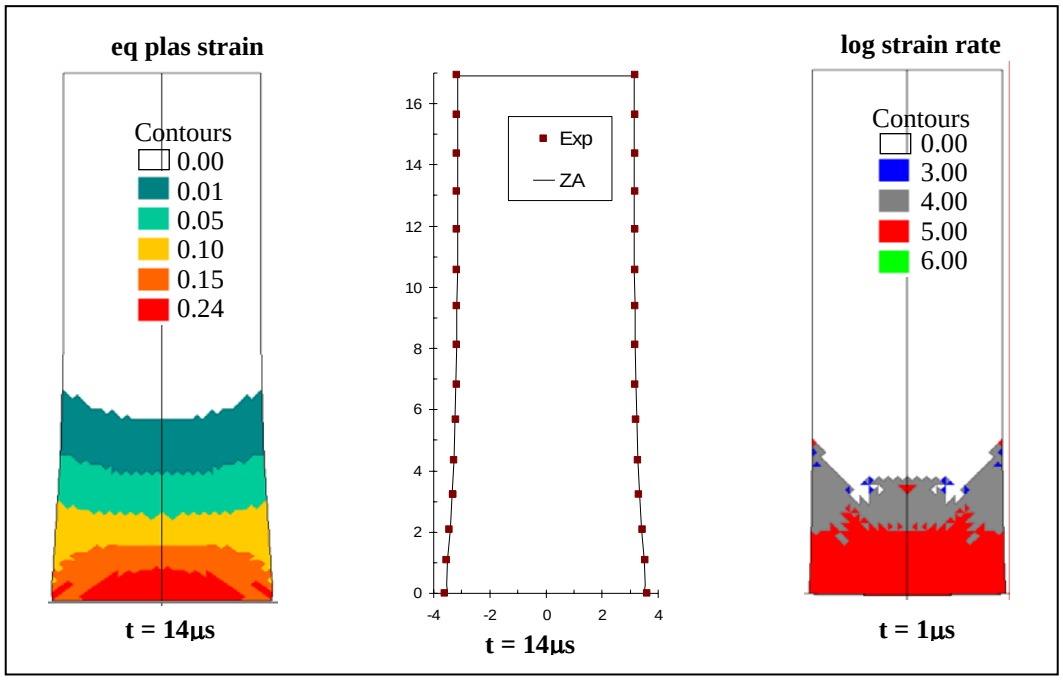

Figure 5. Details of the EPIC simulation of the Taylor anvil test with the use of the modified Zerilli-Armstrong model.

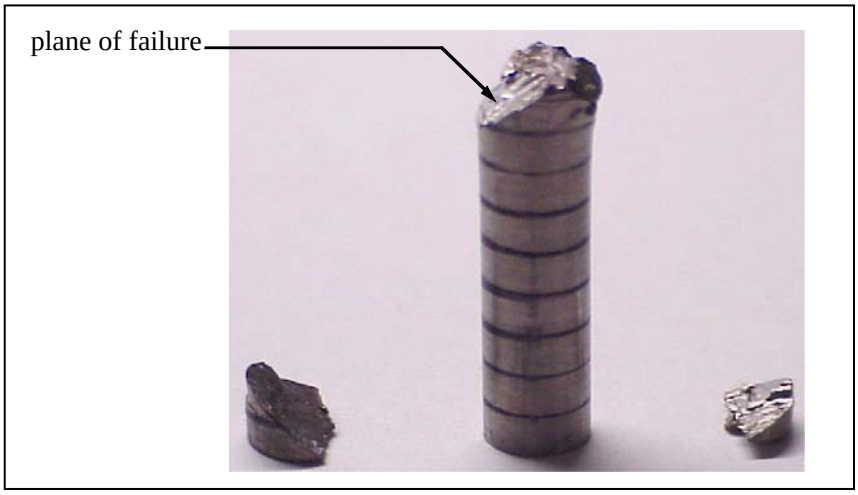

Figure 6. Photograph of shear localized Taylor anvil specimen (impact velocity of 205 m/s).

The modified Zerilli-Armstrong model did not predict localization for this impact velocity with the parameter set of table 2 (see figure 5)[9]. To investigate what would be required for the model to predict localization in the simulation, two excursions were undertaken. In the first, the impact velocity was increased in several sequential steps. Figure 7 shows that localization appears

[9]The prediction of localization in the EPIC simulations of figures 7 and 8 required FAIL=1, whereas the simulation of figure 5 used FAIL=0 (it was the only simulation reported here that used FAIL=0). FAIL=0 will not allow fracture of the material when damage exceeds 1 in the Johnson-Cook fracture model, and FAIL=1 allows degrading of the material strength when damage exceeds 1.

abruptly at 221 m/s, along the plane of failure[10] seen in figure 6. This localization begins when the predominant strain rate drops from a maximum of about $6x10^4$/s to under $2x10^4$/s, roughly equivalent to the value of $\dot{\varepsilon}_\beta$, the lower of the two strain rate constants (table 1). This occurs roughly 9 μs after impact.

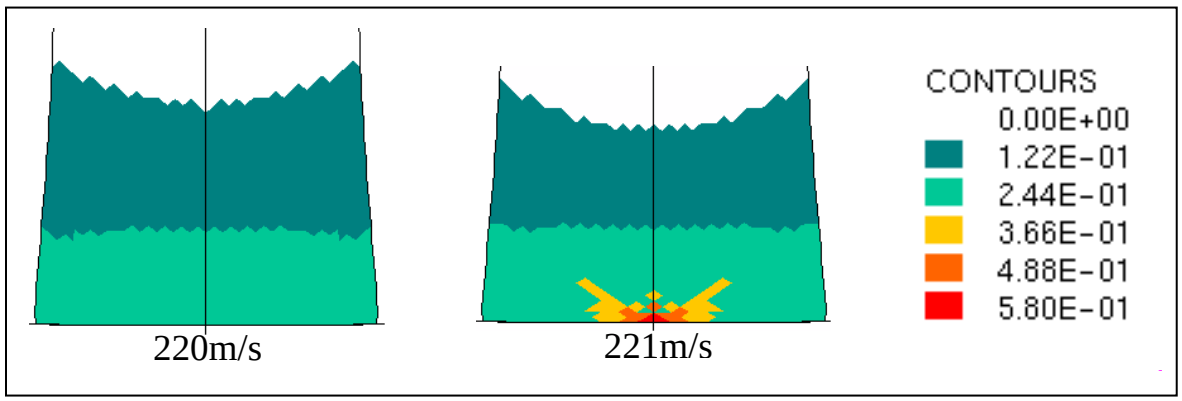

Figure 7. Predicted strain contours showing incipient strain localization in the Taylor anvil test (t = 11 μs is shown; separation from the anvil occurs at abour 14 μs).

At slightly higher velocity, the localization seen in figure 7 extends farther from the impact face, but the 220-m/s case did not show localization at any time (the simulation was run until separation of the specimen from the anvil, 15 μs after impact). The model prediction is consistent with two experimental observations. First is the location and orientation of the localization as seen in figures 6 and 7. Second is the incipient nature of the localization since the model is reasonably predictive of its onset (predicting the onset velocity within about 8% of the experiment). The important achievement is the actual prediction of localization by the strength model.

Variations of β_0 were tested in the second excursion to investigate prediction of localization. Each variation of β_0 was balanced by adjustments in $\dot{\varepsilon}_\beta$ in order to keep β_1 unchanged (in equation 6). If β_0 is increased by just 20%, (β_0 = 1.909e-2, $\dot{\varepsilon}_\beta$ = 1.105e5/s), localization is observed in the simulation (see figure 8). The resulting $\dot{\varepsilon}_\beta$ is on the order of the highest strain rates seen in the Taylor anvil simulation of figure 5. This small change in constants is also consistent with a marginal localization condition seen in the experiments. If β_0 is increased by 50%, (β_0 = 2.387e-2, $\dot{\varepsilon}_\beta$ = 2.022e6/s), localization is more organized and occurs at an earlier time, as seen in figure 8. In this case, $\dot{\varepsilon}_\beta$ is greater than the highest strain rates seen in figure 5, and this is most likely the cause of the improved localization. The deformation of the specimen seemed to be ending at about 9.5 μs (see the inset graph in figure 8). When the localization formed at 11 μs, deformation continued in earnest. The simulations of figure 8 are the only uses of these sets of constants reported here.

Subsequently, the optimization of the model constants was re-run with this latter value of β_0 and $\dot{\varepsilon}_\beta$ fixed (FOM was 1.67%). A simulation using this set of constants did not show localization,

[10]The term “plane” is used loosely in the context of the simulation since the simulation is an axisymmetric calculation.

most likely because of the reduced value of $\dot{\varepsilon}_\alpha$ = 5.13e4 that resulted from the GLO optimiza-tion. This low value (relative to 8.249e5, the value from table 1 used for figure 8) overpowers the increased value of $\dot{\varepsilon}_\beta$ and allows rate hardening to overtake thermal softening too soon.

Prediction of localization thus requires *both* α and β to be positive at the highest strain rates seen in the problem, or at least the combined effect must be positive (e.g., one can be slightly negative).

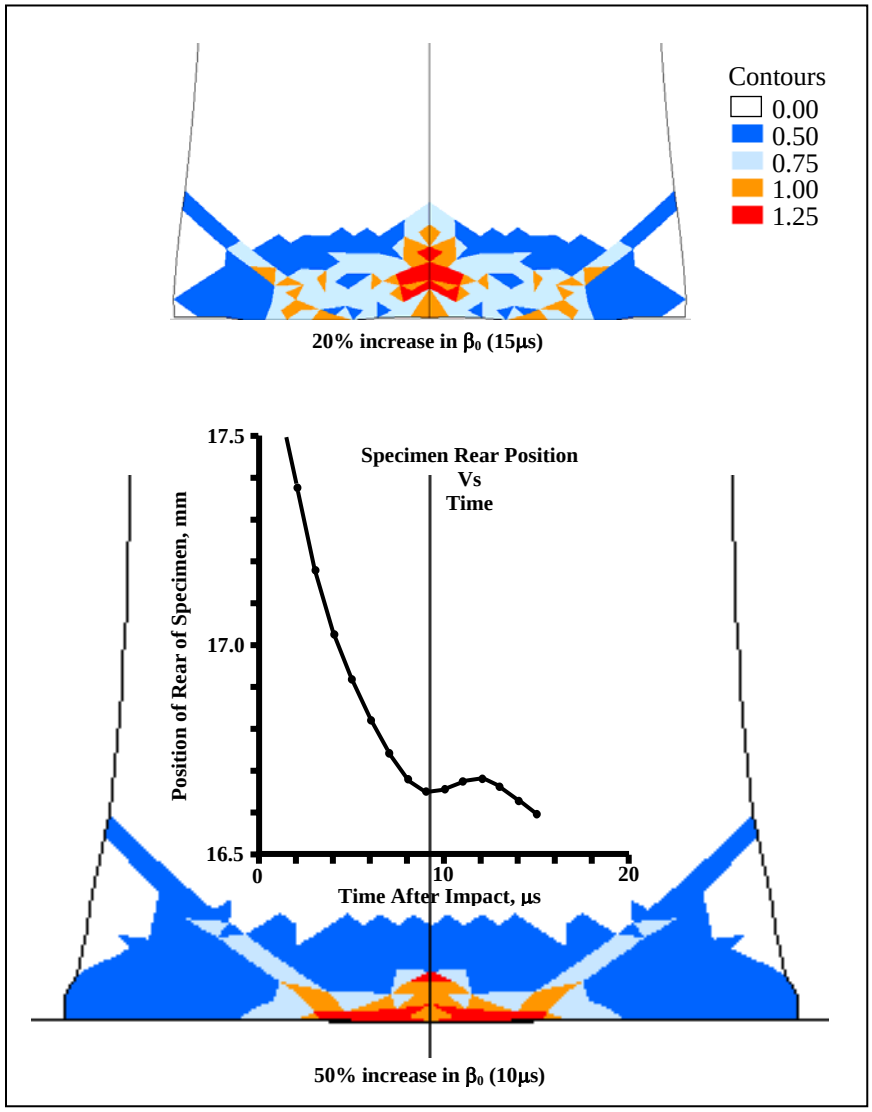

Figure 8. Localization in the Taylor anvil simulation attained when the value of β_0 and $\dot{\varepsilon}_\beta$ was increased.

5.2 Simulation of a V_{50} Experiment

Burkins et al. (*11*) studied the effect of annealing temperature on the ballistic limit velocity of 28.5-mm-thick Ti-6Al-4V plates attacked by a 20-mm steel fragment simulating projectile (FSP). They found the V_{50} of this configuration to be between 1092 m/s and 1141 m/s for the various annealing conditions studied. In those shots that resulted in perforation of the target,

failure of the target was observed to occur by plugging (i.e., shearing out of a cylindrical plug of target material ahead of the penetrator). In those shots that resulted in incomplete penetration, shear bands were often observed parallel and perpendicular to the direction of fire. Figure 9 shows a typical example (from reference *11*; reprinted by permission of the principal author).

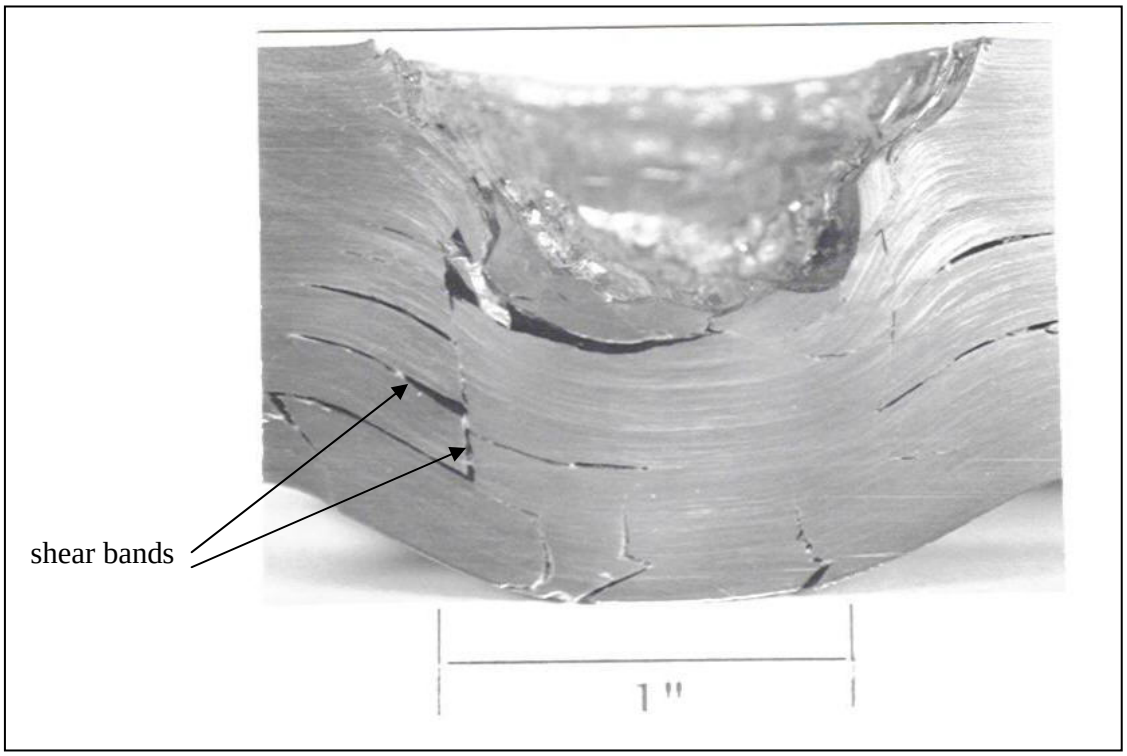

Figure 9. Sectioned view of the impact crater and remaining plate from a V_{50} experiment (taken from reference (*11*); reprinted by permission). (Striking velocity was 1106 m/s, near the limit velocity.)

The test configuration was simulated in axisymmetric EPIC with the use of a 20-mm-long by 20-mm-diameter steel cylinder (10 crossed elements across the FSP radius) and the model of equation 9 and table 1. Results of two significant simulations are shown in figure 10. At 1020 m/s, the FSP was unable to perforate the target (notice that it has begun to rebound out of the target at 120 μs), although some spalling occurs on the rear surface. At 1040 m/s, spalling also occurs at the early time, but perforation is clearly occurring at the late time. Thus, a predicted V_{50} of approximately 1030 m/s is indicated, which is within 6% to 11% of the experimental values.

The most striking feature in figure 10 is the appearance of strain localization at the 1040-m/s impact velocity. Thus, the threshhold perforation at 1040 m/s is accomplished by strain localization in the target and plugging of the rear portion of the target, consistent with what was observed experimentally by Burkins et al. (*11*, *15*). The simulation even shows a small amount of the perpendicular shear banding, which indicates that the origin of this failure seen in the experiments (figure 9) is more than just metallurgical (e.g., from the rolling of the plates during processing).

Strain rate contours in figure 10 show that the highest rates in the 1040-m/s case are about 10^5/s, a strain rate slightly greater than $\dot{\varepsilon}_\beta$ and slightly less than $\dot{\varepsilon}_\alpha$ (table 1).

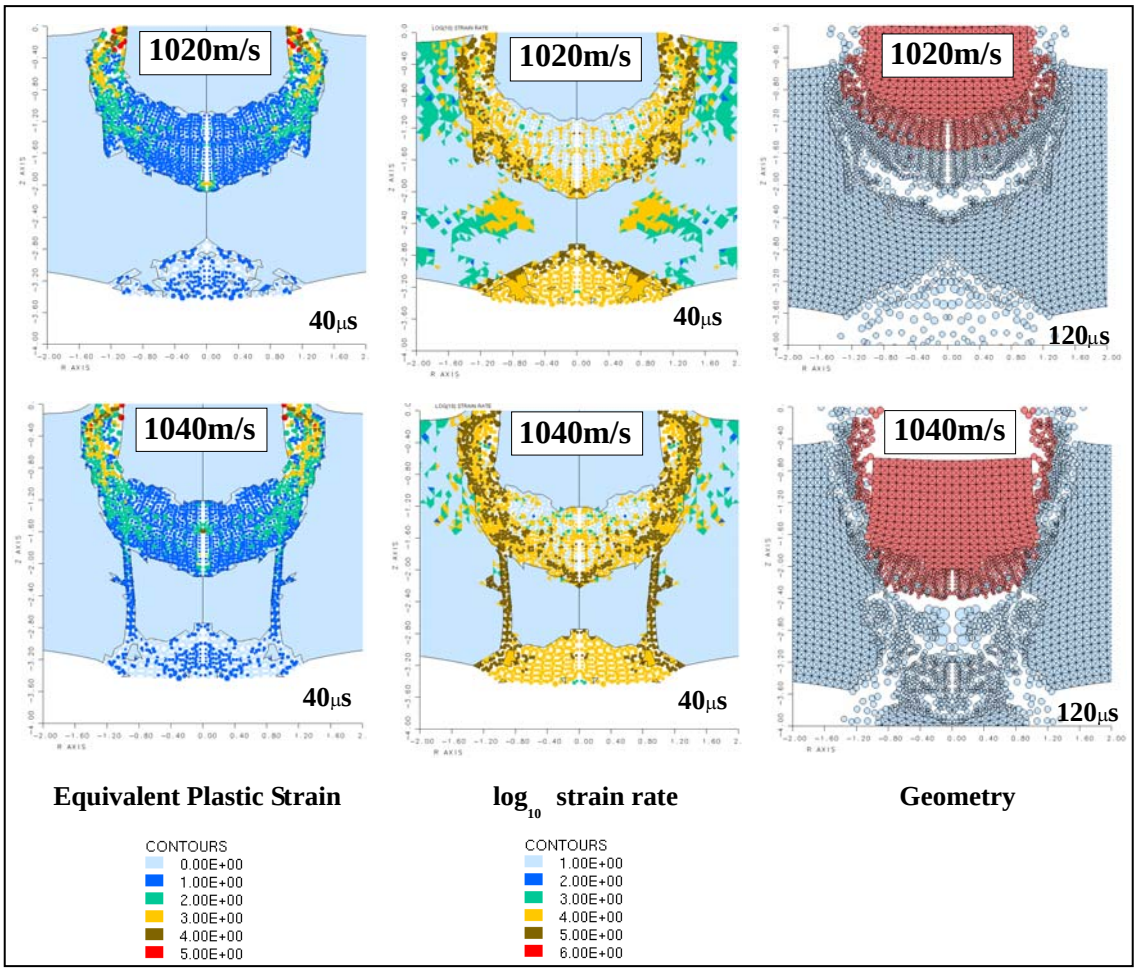

Figure 10. Localization and plugging in simulations of V_{50} experiments with the use of equation 9 to model the target. (Experimental V_{50} for this target was approximately 1100 m/s.)

When the impact velocity was increased to 1300 m/s, a second cylindrical localization band appeared at a slightly larger diameter than the primary band (that of figure 10). The slight perpendicular shear banding observable in figure 10 for the 1040-m/s case became slightly more pronounced. At 1400 m/s, the localization and plugging continued to mark the failure process, 55and the small perpendicular shear band became slightly more pronounced. The plugging and localization continued until at least 1500 m/s, but at a velocity of 2000 m/s, no plugging or localization was observed—just massive deformation and failure as the FSP pushed violently through the target.

For comparison, the Burkins' et al. V_{50} experiment was modeled with the Zerilli-Armstrong bcc model from reference *7*. The V_{50} for the bcc model was about 1400 m/s, a significant error. Even though that model did not include any explicit measures to model localization as does

equation 9, the bcc model did show the beginning of localization. Figure 11 shows a good example. However, the localization seen in figure 11 did not grow at times beyond 40 μs, and at higher velocity, the localization was swamped by widespread failure of the material ahead of the penetrator. Thus, the localization did not develop into plugging as seen in the experiment (figure 9) and in the simulation (figure 10). One reasonable interpretation of this outcome is that the coupling of strain rate hardening and thermal softening is well represented in both the bcc model and the present model (the coupling is in the exponential terms, which are similar in the two models), but the Taylor strain hardening of the bcc model inhibited growth of the localization, whereas the strain function of the present model favors that growth.

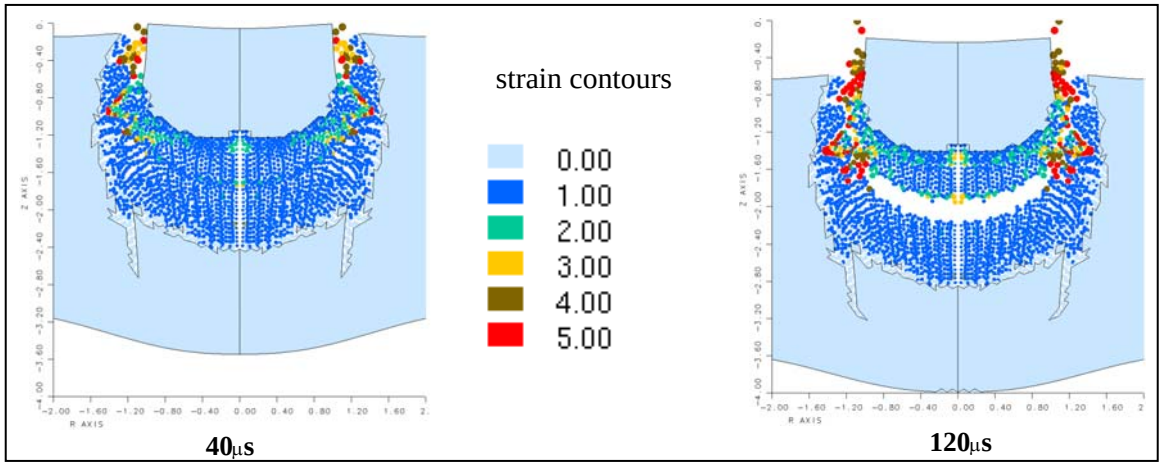

Figure 11. Nascent localization with the Zerilli-Armstrong bcc model in simulations of V_{50} experiments (1200-m/s impact velocity shown).

5.3 Simulation of Ti-6Al-4V on Ti-6Al-4V Penetration Experiments

Meyer and Kleponis (*7*) performed penetration experiments using semi-infinite targets fabricated from the Ti-6Al-4V material, impacted by penetrators made of the same material. A summary of a portion of their results is shown in figure 12. Their experimental results are shown as the solid symbols, and the line is a fit to the data. The open triangles show the results of 3-D CTH simulations using the Zerilli-Armstrong bcc model, included here for comparison. The open squares show the results for axisymmetric EPIC (five crossed elements across the penetrator radius) with the current model. Predicted depth of penetration (DOP) is reasonably accurate from 1200 m/s to 1600 m/s, but the error is substantial at 2000 m/s. Maximum strain rates at this impact velocity are greater than 10^6 in the target, higher than the data used to calibrate the model, and 10^5 in the penetrator, slightly higher than the data. Maximum rates were about one-third as high at an impact velocity of 1600 m/s. Efforts are under way to install this model into CTH in order to conduct 3-D simulations for direct comparison to the bcc model predictions.

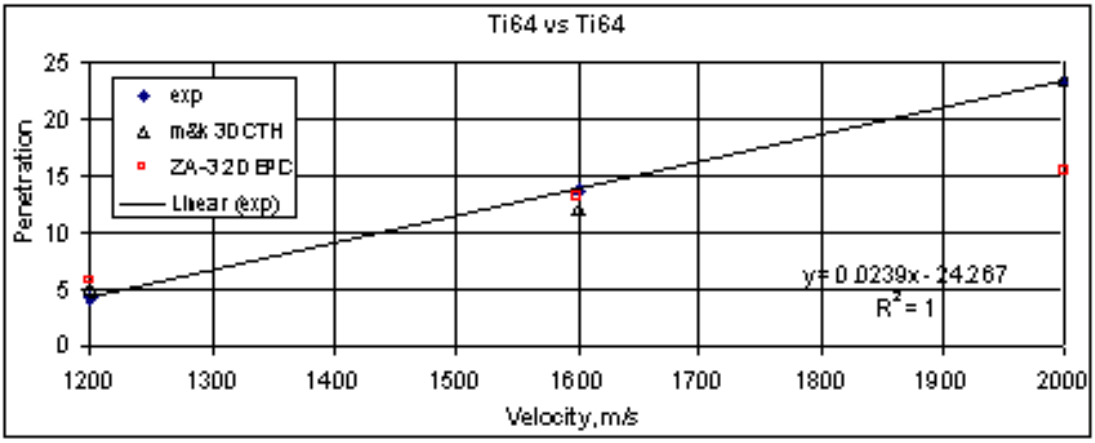

Figure 12. Simulation results compared to experiment and 3-D CTH with an earlier ZA model.

5.4 Simulation of the Penetration of the 190W Round Into Ti-6Al-4V

Gooch and Burkins (*16*) studied the performance of Ti-6Al-4V attacked by various penetrators, including the 190W, which is an l/d=20, 93% tungsten rod, 190.5 mm long. Impact velocities for the 190W were between 950 m/s and 1700 m/s. Gooch and Burkins recorded the DOPs and fit those data with an analytical function, plotted as the solid line in figure 13. Plotted as open symbols in figure 13 are results of axisymmetric EPIC simulations (five crossed elements across the penetrator radius) with three different strength models for the Ti-6Al-4V. The 190W was modeled with the Johnson-Cook strength model using constants from reference *4* (except the yield strength here was 1.17 GPa), the Mie-Gruneisen equation of state (EOS), and the Johnson-Cook fracture model. EPIC library constants were used for the EOS and fracture model.

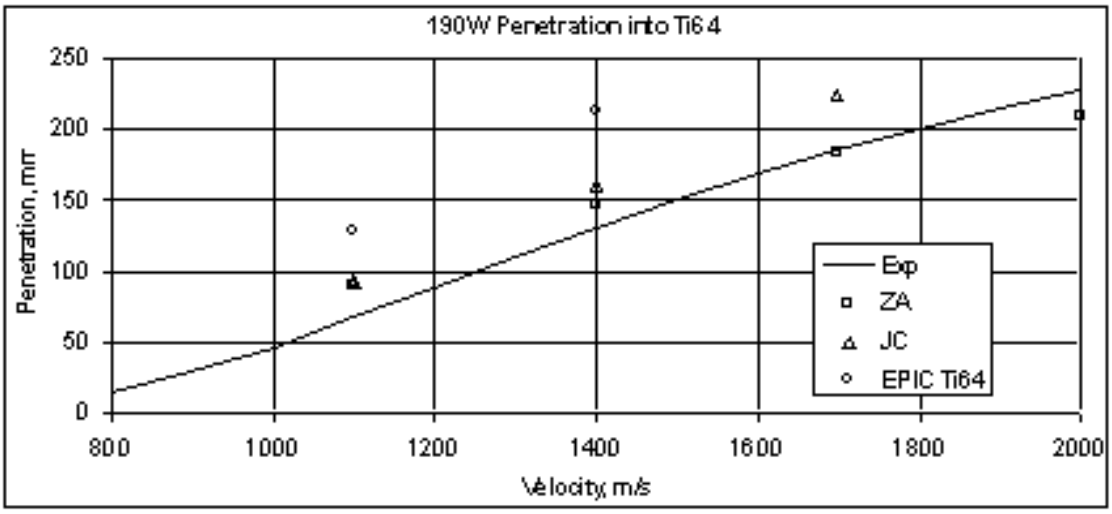

Figure 13. Axisymmetric EPIC simulation results for the current model compared to experiment and other models.

Predictions of depth of penetration into the Ti-6Al-4V were inaccurate when the Ti-6Al-4V was modeled with the Johnson-Cook strength model using constants from the EPIC library (open

circles in figure 13). This shows the error of using that constant set to model the low cost Ti-6Al-4V material. The 300-mm-thick target was perforated at 1700 m/s with that model. When the set of constants in table 2 is used with the Johnson-Cook strength model, results are much improved (open triangles in figure 13), although inaccuracy increases as impact velocity is increased. Results are much better over the range of 1100 m/s to 2000 m/s when the modified Zerilli-Armstrong model is used with constants from table 1.

6. Conclusion

The Zerilli-Armstrong hcp model was modified and fit to high rate Hopkinson Bar data. The fit to the data was very good. The model was installed into EPIC and performed well in a varied series of axisymmetric simulations. It did not perform well for the case of a Ti-6Al-4V penetrator impacting a block of Ti-6Al-4 V at 2000 m/s.

7. Recommendation

Because CTH is used for large scale penetration simulations at ARL, the model should be installed into CTH and tested in the same series of simulations with 3-D CTH. Numerical effects of the axisymmetric calculations (e.g., anomalies on the axis of symmetry) in EPIC may have affected the high-velocity EPIC penetration simulations, and this provides additional motivation to examine the model's performance in 3-D CTH.

8. References

1. Casem, D. *High Strain Rate Compression of Ti-6Al-4V*; technical report; U.S. Army Research Laboratory: Aberdeen Proving Ground, MD, to be published.

2. Johnson, G. R.; Beissel, S.R.; Stryk, R.A.; Gerlach, C.A.; Holmquist, T.J. *User Instructions for the 2003 Version of the EPIC Code*; Final Report, Contract F08630-02-M-0077; Air Force Research Laboratory, Eglin AFB, FL, October 2003.

3. McGlaun, J. M.; Thompson, S.L. CTH: A Three-Dimensional Shock Wave Physics Code. *International Journal of Impact Engineering* **1990**, *10*, 351-360.

4. Johnson, G. R.; Cook, W. H. A Constitutive Model and Data for Metals Subjected to Large Strains, High Strain Rates, and High Temperatures. *Proceedings of the 7th International Symposium on Ballistics*, The Hague, The Netherlands, April 1983, pp. 541-547.

5. Zerilli, F. J.; Armstrong, R. W. Dislocation-mechanics based constitutive relations for material dynamics calculations. *J. Appl. Phys.* **1 March 1987**, *61* (5), 1816-1825

6. Zerilli, F. J.; Armstrong, R. W. Constitutive Relations for the plastic Deformation of Metals, in High-Pressure Science and Technology - 1993, edited by Schmidt, S. C., Shaner, J. W., Samara, G. A., and Ross, M. AIP Press, New York, 1994, pp 989 - 992.

7. Meyer, H. W.; Kleponis, D. S. Modeling the High Strain Rate behavior of Titanium Undergoing Ballistic Impact and Penetration. *International Journal of Impact Engineering* **2001**, *26*, 509-521.

8. Zerilli, F. J.; Armstrong, R. W. Constitutive Relations for Titanium and TI-6AL-4V. *Proceedings of the American Physical Society Topical Group on Shock Compression of Condensed Matter Conference*, 1995, pp 315-318.

9. Zerilli, F. J.; Armstrong, R. W. Constitutive Equation for HCP Metals and High Strength Alloy Steels. AD- Vol. 48, High Strain Rate Effects on Polymer, Metal and Ceramic Matrix Composites and Other Advanced Materials, ASME 1995, pp 121-126.

10. Zerilli, F. J.; Armstrong, R. W. Dislocation Mechanics Based Constitutive Equation Incorporating Dynamic recovery and Applied to Thermomechanical Shear Instability. *Proceedings of the American Physical Society Topical Group on Shock Compression of Condensed Matter Conference*, 1997, pp 215-218.

11. Burkins, M. S.; Love, W. W.; Wood, J. R. *Effect of Annealing Temperature on the Ballistic Limit Velocity of Ti-6Al-4V ELI*; ARL-MR-359; U.S. Army Research Laboratory: Aberdeen Proving Ground, MD, August 1997.

12. Taylor, G. I. Proceedings of the Royal Society A145, 362 (1934).

13. Murphy, M. J. *GLO - Global Local Optimizer User's Manual*; UCRL-MA-133858; Dec 2003.

14. Casem, D.; Meyer, H.; Cardenas-Garcia, J. Re-examining the Taylor Impact Test Using a Finite-Element-Based Inverse Problem Methodology. *Proceedings of the 2005 Society for Experimental Mechanics Annual Conference and Exposition on Experimental and Applied Mechanics*, Portland, Oregon, June 2005.

15. Burkins, M. S.; Hansen, J. S.; Paige, J. I.; Turner, P. C. *The Effect of Thermo-mechanical Processing on the Ballistic Limit Velocity of Extra Low interstitial Titanium Alloy Ti-6Al-4V*; ARL-MR-486; July 2000.

16. Gooch, W. A.; Burkins, M. S. *A Ballistic Evaluation of Ti-6Al-4V vs. Long Rod Penetrators*; NATO RTO-MP-069(II); Applied Vehicle Technology Panel Specialists' Meeting, Loen, Norway, 7-11 May 2001 (published March 2003).

NO. OF COPIES ORGANIZATION

1 (PDF ONLY) DEFENSE TECHNICAL INFORMATION CTR
DTIC OCA
8725 JOHN J KINGMAN RD
STE 0944
FORT BELVOIR VA 22060-6218

1 US ARMY RSRCH DEV & ENGRG CMD
SYSTEMS OF SYSTEMS INTEGRATION
AMSRD SS T
6000 6TH ST STE 100
FORT BELVOIR VA 22060-5608

1 DIRECTOR
US ARMY RESEARCH LAB
IMNE ALC IMS
2800 POWDER MILL RD
ADELPHI MD 20783-1197

1 DIRECTOR
US ARMY RESEARCH LAB
AMSRD ARL CI OK TL
2800 POWDER MILL RD
ADELPHI MD 20783-1197

2 DIRECTOR
US ARMY RESEARCH LAB
AMSRD ARL CS OK T
2800 POWDER MILL RD
ADELPHI MD 20783-1197

ABERDEEN PROVING GROUND

1 DIRECTOR
US ARMY RSCH LABORATORY
ATTN AMSRD ARL CI OK (TECH LIB)
BLDG 4600

NO. OF COPIES ORGANIZATION

36 DIRECTOR
US ARMY RSCH LABORATORY
ATTN AMSRD ARL WM T WRIGHT
AMSRD ARL WM TA M BURKINS
C HOPPEL E HORWATH
D KLEPONIS B LEAVY
J RUNYEON S SCHOENFELD
AMSRD ARL WM TB R SKAGGS
AMSRD ARL WM TC R ANDERSON
T FARRAND K KIMSEY
D SCHEFFLER S SCHRAML
AMSRD ARL WM TD S BILYK
T BJERKE D CASEM
J CLAYTON D DANDEKAR
M GREENFIELD Y HUANG
K IYER B LOVE H MEYER (6 CYS)
R MUDD E RAPACKI
M RAFTENBERG M SCHIEDLER
S SEGLETES T WEERASOORIYA
AMSRD ARL WM MD B CHEESEMAN